A numerical study on the effect of asymmetry on underwater noise emission in offshore monopile installation

Molenkamp, Timo; Tsouvalas, Apostolos; Metrikine, Andrei

DOI
10.1016/j.oceaneng.2024.117351

Publication date
2024

Document Version
Final published version

Published in
Ocean Engineering

Citation (APA)
Molenkamp, T., Tsouvalas, A., & Metrikine, A. (2024). A numerical study on the effect of asymmetry on underwater noise emission in offshore monopile installation. *Ocean Engineering*, *299*, Article 117351. https://doi.org/10.1016/j.oceaneng.2024.117351

Ocean Engineering 299 (2024) 117351

Contents lists available at ScienceDirect

Ocean Engineering

journal homepage: www.elsevier.com/locate/oceaneng

A numerical study on the effect of asymmetry on underwater noise emission in offshore monopile installation

Timo Molenkamp *, Apostolos Tsouvalas, Andrei Metrikine

Faculty of Civil Engineering and Geosciences, Delft University of Technology, Stevinweg 1, Delft, 2628 CN, Netherlands

ARTICLE INFO

Keywords:
Underwater noise
Pile driving
Asymmetric noise field
Inclined pile

ABSTRACT

Offshore wind energy holds significant promise as a solution in the energy transition. However, installing offshore pile foundations can generate substantial levels of underwater noise, posing potential risks to marine life. This paper examines the influence of asymmetric impact forces and pile inclination on producing underwater noise and seabed vibrations based on cases of a small- and large-diameter monopile. The study focuses on scenarios involving inclined and eccentric forces and tilted piles. The analysis reveals that non-symmetrical conditions significantly impact the sound pressure levels around the ring frequency of the pile due to various noise generation mechanisms. However, it is observed that the vertical component of the impact force predominantly contributes to the generation of underwater noise, primarily due to its considerably higher amplitude.

1. Introduction

Offshore wind energy is an essential renewable energy source, but the construction of offshore wind turbines can have significant environmental impacts. The increasing size of monopiles to support the increasingly large offshore wind turbines presents several challenges. According to Sunday and Brennan (2021), these challenges include assessing and controlling construction peak noise levels, managing noise exposure levels, addressing excessive pile inclination, and preventing plastic deformation of the thin-shell pile head caused by the more significant hammer force required for pile driving.

High underwater sound levels generated during the installation of monopile foundations with impact pile driving can disturb the behaviour of marine life several kilometres away from the site (Dahl et al., 2014; Madsen et al., 2006), and it can lead to physical harm and even fatal injury of underwater mammals near the driving site (Southall et al., 2019).

Though more silent pile driving methods are under development (Tsetas et al., 2023), accurate predictions are required to forecast the underwater noise field caused by offshore pile driving. As a result, several models have been developed in the past decade. Early noise prediction models employed an acoustic fluid representation of the sediment, focussing on the radiation of the Mach wave (Reinhall and Dahl, 2011; Lippert and Lippert, 2012; Zampolli et al., 2013). Second-generation models included an elastic description of the sediment (Tsouvalas and Metrikine, 2014; Göttsche et al., 2015; Fricke and Rolfes, 2015; Jiang et al., 2022).

Peng et al. (2021a) improved the modelling of the propagated sound field using Green's functions, while Lippert et al. (2018) presented a simplified approach based on transmission losses. Last, semi-empirical models are developed, providing scaling laws on hammer properties, pile dimensions and water depth (von Pein et al., 2022).

However, several open challenges remain, including developing models suitable for vibratory pile driving, noise mitigation systems, uncertainty analysis and non-symmetric noise fields (Tsouvalas, 2020). Recently, steps have been taken to understand noise generated during vibratory pile driving (Molenkamp et al., 2023), model air-bubble curtains to mitigate high noise levels (Peng et al., 2021b) and propagate mitigated noise fields (Jestel et al., 2021).

Inclined forces have earlier been addressed in Tsouvalas and Metrikine (2013) and Deng et al. (2016) via simplified acoustic models representing soil with springs. However, quantifying the effect on noise emission has not been systematically studied. Wilkes and Gavrilov (2017) modelled and studied the sound radiated from impact-driven raked piles, where the raked piles are installed under an angle of 14.5° and have significantly smaller dimensions than monopile foundations. The soil is modelled herein as an acoustic fluid, disregarding pile-soil interaction.

This paper focuses on the effect of unintended non-symmetric sound fields generated during impact piling of monopile foundations for wind farms. Specifically, the cases with an inclined force, an eccentric force and a tilted pile are studied. Since measurements sometimes show

* Corresponding author.
E-mail address: t.molenkamp@tudelft.nl (T. Molenkamp).

https://doi.org/10.1016/j.oceaneng.2024.117351
Received 11 September 2023; Received in revised form 17 November 2023; Accepted 28 February 2024
Available online 10 March 2024

substantial azimuthal variation of the acoustic field, the impact of non-symmetries in the force and geometry on noise levels should be investigated.

This paper quantifies and explains the effect of non-symmetric force excitations on underwater acoustics noise fields, focusing on inclined forces, eccentric forces, and an inclined pile. The effects are studied using frequency domain analysis based on the case of a small- and large-diameter monopile. The paper provides physical explanations of the results and offers advice for engineering applications.

A COMSOL Multiphysics® FEM model is built to model the pile and its vicinity, predicting sound pressure levels, sound exposure levels, and peak pressures in the frequency domain. The model description is provided in Section 2, containing governing equations and modelling assumptions. Section 3 examines two case studies on installing a small and large-diameter monopile. The small pile is modelled to compare conclusions with Deng et al. (2016) and can represent a pin pile. The large-diameter monopile described by Peng et al. (2021a) is modelled to verify the conclusions on a practical scale. Lastly, the conclusions are given in Section 4.

2. Model description

A model is created in COMSOL Multiphysics® (2022) to evaluate the non-symmetric excitation forces. COMSOL Multiphysics® is a finite element package often used for near-field noise generation, i.e. the first tens of meters. In the Compile benchmark case (Lippert et al., 2016), four out of seven participants used COMSOL Multiphysics® as a noise generation model, and it has been validated against data by and validated against measurements (Zampolli et al., 2013; Reinhall and Dahl, 2011). The disadvantage of a finite element package is the computational expenses; therefore, separate models are used for far-field propagation, i.e., hundreds of meters to kilometres, and the software is unsuitable for uncertainty analysis. The near-field results can be propagated with different methods, such as the wave number integration, normal modes or parabolic equation method, to predict the acoustic far-field. To reduce computational costs, mode extension around the circumferential azimuth is used, reducing the discretization from 3D to 2D for the cases of inclined and eccentric forces. The tilted pile is modelled in 3D with significant computational costs.

The model geometry presented in Fig. 1 shows the model domains and boundaries. Ω_f indicates the fluid domain, modelled with acoustic elements and is described by:

$$\nabla \cdot \left(\nabla p_{\mathrm{f}}(r,\theta,z) - \boldsymbol{q}_{\mathrm{f}}(r,\theta,z)\right) + \frac{\omega^2}{c_{\mathrm{f}}} p_{\mathrm{f}}(r,\theta,z) = -\rho_{\mathrm{f}} Q_{\mathrm{f}}(r,\theta,z) \tag{1}$$

with pressure field $p_{\mathrm{f}}(r,\theta,z)$, $Q_{\mathrm{f}}(r,\theta,z)$ being a monopole domain source and $\boldsymbol{q}_{\mathrm{f}}(r,\theta,z)$ contains dipole domain sources. The parameters ρ_{f}, c_{f} and ω are the fluid density, fluid wave speed and angular frequency, respectively. The pile and soil domains, Ω_p and Ω_s are modelled with solid elements described by:

$$\nabla \cdot \boldsymbol{\sigma}_{\mathrm{s}}(r,\theta,z) + \boldsymbol{F}_{\mathrm{s}}(r,\theta,z) = -\rho_{\mathrm{s}}\omega^2 \boldsymbol{u}_{\mathrm{s}}(r,\theta,z) \tag{2}$$

with stress vector $\boldsymbol{\sigma}_{\mathrm{s}}(r,\theta,z)$, displacement vector $\boldsymbol{u}_{\mathrm{s}}(r,\theta,z)$ and force vector $\boldsymbol{F}_{\mathrm{s}}(r,\theta,z)$ containing the external hammer forces (F_{ext}) at the top of the pile; ρ_{s} is the solid density.

The 2D axisymmetric model has a symmetry axis at $r = 0$, i.e. boundary Γ_0. Boundaries $\Gamma_{\mathrm{f}\infty}$ and $\Gamma_{\mathrm{s}\infty}$ are prescribed by Sommerfeld's radiation condition and modelled in COMSOL Multiphysics® as Cylindrical Wave Radiation and Low-reflecting boundaries, respectively. The sea surface, $\Gamma_{\mathrm{f}0}$, is modelled as a pressure release boundary, i.e. $p_{\mathrm{f}} = 0$. The interfaces between pile and fluid, and soil and fluid, Γ_{fs} and Γ_{f} are modelled with Acoustic-Structure Boundary conditions, prescribing continuity of normal displacements and pressure and allowing no shear stresses. The pile-soil interface needs no specific description since both are modelled with the same type of elements with different material properties. Pile and soil are connected monolithically, i.e. no pile slip

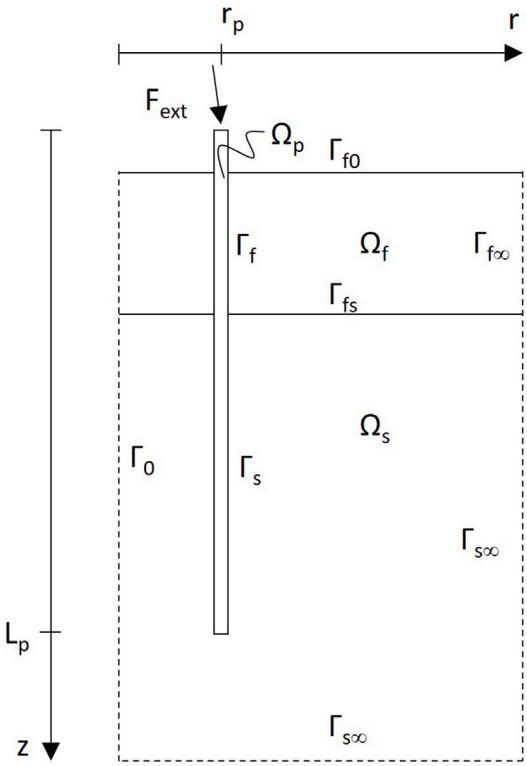

Fig. 1. Model geometry.

or separation is allowed relative to the soil. The model is truncated five m below the bottom of the pile and at $r = 75$ and $r = 150$ m for the small and large piles, respectively. A frequency-dependent adaptive mesh size is used that guarantees five elements per wavelength.

The 3D model is similar to the 2D axisymmetric model, but the entire 3D domain is modelled, and the axis of symmetry is removed. The pile is rotated around the y-axis halfway through its length. A symmetry plane boundary is introduced at $y = 0$. The domain is truncated at $r = 50$ m to reduce computation costs as computational costs grow exponentially with an extended domain in r. The domain truncations are considered sufficient (compared to 6.5 m in Wilkes and Gavrilov (2017)) to describe the noise generation mechanism, whereas propagation can be obtained by other than FEM methods.

This paper considers two types of non-symmetric forces: An inclined force and an eccentric force. The relation between the vertical and horizontal comments of the force, $F_z(t)$ and $F_x(t)$, are found via:

$$F_x(t) = \tan(\alpha) F_z(t), \qquad \rightarrow \qquad F_{\mathrm{ext}} = \sqrt{F_x^2 + F_z^2} \tag{3}$$

with α being the time-independent angle of inclination. During installation, the maximally allowable tilt at the seabed level is 0.25 degree (Veritas, 2004), and due to modern motion-compensated pile grippers, the monopile installation happens almost vertically. This paper assumes an angle of three degrees, which is assumed to be a practical upper limit. Therefore, the $F_x(t)$ is approximately 5% of $F_z(t)$.

The eccentric force induces a moment around the y-axis next to the vertical force. The moment $M_y(t)$ is found via:

$$M_y(t) = \beta r_{\mathrm{p}} F_z(t) \tag{4}$$

with a relative eccentricity $\beta = \epsilon / r_{\mathrm{p}}$ and ϵ being the absolute eccentricity. This paper assumes that the eccentricity is proportional to 5% of the pile's radius, again assuming to be an extreme case. These forces translate to distributed loads on top of the pile per azimuthal mode number via:

$$q_{z0}(t) = \frac{1}{2\pi r_{\mathrm{p}}} F_z(t) \tag{5}$$

Table 1
Small diameter pile geometry and material properties (Deng et al., 2016).

Parameter		unit
Pile Youngs modulus [E_p]	210	GPa
Pile Poison's ratio [ν_p]	0.28	–
Pile density [ρ_p]	7800	kg m^{-3}
Structural damping [ν_p]	0.002	–
Pile length [L_p]	28	m
Pile radius [r_p]	1	m
Pile thickness [h_p]	0.02	m
Pile soil penetration	10	m
Fluid wave speed [c_f]	1500	m s^{-1}
Fluid density [ρ_f]	1000	kg m^{-3}
Water depth	8	m
Soil Youngs modulus [E_s]	50	MPa
Soil Poison's ratio [ν_s]	0.40	–
Soil density [ρ_p]	1600	kg m^{-3}

$$q_{r1}(t) = \frac{1}{2\pi r_p} F_x(t)\cos(\theta) \tag{6}$$

$$q_{\theta 1}(t) = -\frac{1}{2\pi r_p} F_x(t)\sin(\theta) \tag{7}$$

$$q_{z1}(t) = \frac{1}{\pi r_p^2} M_y(t)\cos(\theta) \tag{8}$$

The effect of each force component is examined in the case studies hereafter.

The case with the tilted pile assumes a tilt of three degrees; this limit case is reviewed to find pressure level differences and seabed vibrations on both sides of the pile. The force is assumed to be in parallel with the pile.

3. The non-symmetric noise field

The non-symmetric noise field is examined for the case of a small- and large-diameter monopile taken from Deng et al. (2016) and Peng et al. (2021a), respectively. In both cases, the effect of non-symmetry of noise is examined; the conclusions are compared for the small monopile with those of Deng et al. (2016). The physical explanation of the noise generation is accomplished based on the large monopile case. A frequency domain analysis is performed, and the time domain response is retrieved using an inverse FFT. To quantify the noise emission, the sound exposure levels, L_E, sound pressure levels, L_p and the peak sound pressure level, L_{peak} are calculated by the definition of ISO (2017):

$$L_E = 10\log_{10}\left(2\int_0^\infty \frac{|p_f(f)|^2}{p_0^2}\mathrm{d}f\right) \tag{9}$$

$$L_P = 20\log_{10}\left(\frac{p_{rms}(f)}{p_0}\right) \tag{10}$$

$$L_{peak} = 20\log_{10}\left(\frac{p_{peak}}{p_0}\right) \tag{11}$$

in which real mean square pressure $p_{rms}(f) = \frac{1}{\sqrt{2}}|p_f(f)|$ and peak pressure $p_{peak} = \max(|p_f(t)|)$. The reference pressure $p_0 = 1$ μPa for underwater acoustic calculations. The force transfer functions are defined by:

$$T_{p_f,F_\alpha} = \frac{p_f}{F_\alpha} \tag{12}$$

with F_α being F_z, F_x or M_y.

3.1. Small-diameter pile

Deng et al. (2016) show the case of a two meter diameter monopile of 28 m length partially driven in the soil. Piles of these dimensions are relatively small in the current offshore wind industry but are used for jacket foundations. The corresponding ring frequency is $f_{ring} \approx 857$ Hz. The water depth is shallow, resulting in a cut-off frequency of the first propagating mode of about 47 Hz. Further material and geometry properties are summarized in Table 1.

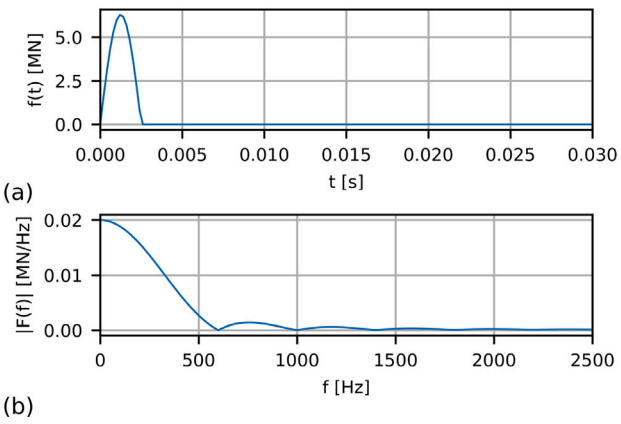

Fig. 2. (a) Time and (b) frequency domain representation of the force on the small-diameter pile (Deng et al., 2016).

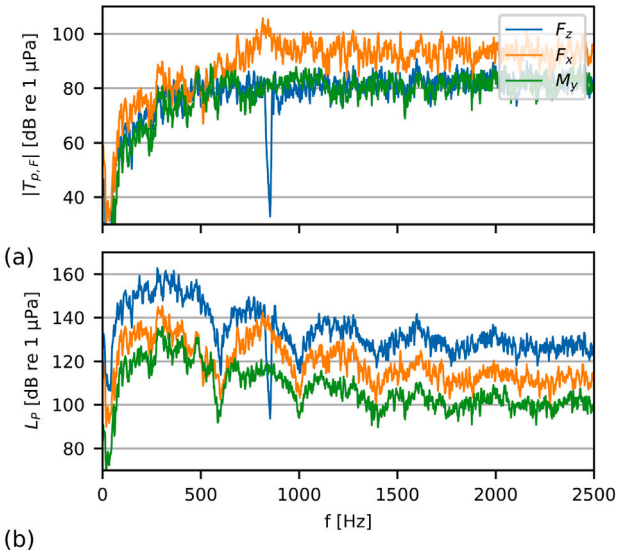

Fig. 3. (a) Absolute value of the transfer functions and (b) sound pressure levels for a vertical load, horizontal load and moment on top of the pile at $z = 4$ m and $r = 25$ m.

The external load on top of the pile is described by:

$$F_{ext}(t) = F_0 \sin\left(\frac{\pi t}{\tau}\right) \qquad 0 < t < \tau \tag{13}$$

with $F_0 = 1$ MN m^{-1} and $\tau = 2.5$ ms. Fig. 2a shows the time signature of the applied force while Fig. 2b shows the amplitude spectrum of the force. Frequencies up to 2500 Hz with a stepsize of 1 Hz are included in the frequency response analysis.

The absolute value of the frequency response transfer functions in Fig. 3 shows the pressure levels at $z = 4$ m and $r = 25$. The transfer functions are plotted on a decibel scale after substitution in Eq. (10). The transfer function shows almost no sound propagation below ≈37.5 Hz, the cut-off frequency of the fluid and around ≈857 Hz, the ring frequency of the pile.

The ring frequency of the pile indicates the frequency at which the wavelength is equal to the circumference of the pile. The modal density around this frequency is high (Leissa, 1973). The vertical group velocity of waves close to the ring frequency is almost zero. Thus, almost no energy propagates downwards the pile from the hammer impact location. This is further discussed in Section 3.2.

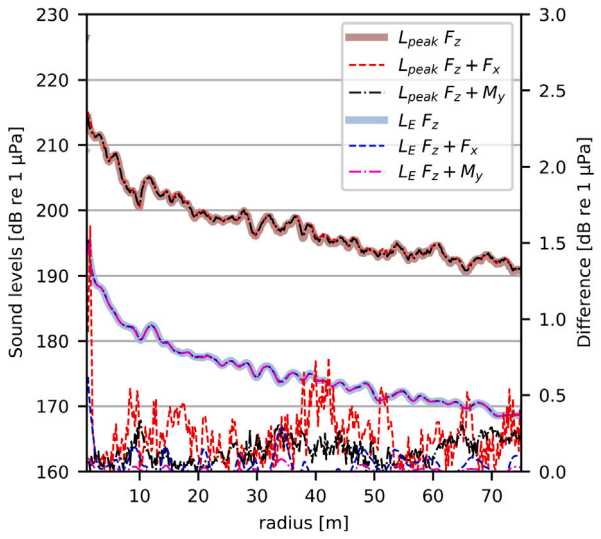

Fig. 4. Peak pressure and sound exposure levels at 4 m depth to radius caused by the vertical, inclined, and eccentric load on the left axis and the dB difference compared to only the vertical load on the right axis.

The sound waves generated by a horizontal force or a moment do not propagate below the fluid's cut-off frequency but propagate at the pile's ring frequency, while the ring frequency corresponds solely to the axisymmetric shell. The absolute value of the transfer functions of a horizontal load is significantly higher than those of a vertical load. Nonetheless, the sound pressure levels, shown in Fig. 3b, are significantly lower compared to the vertical load since the amplitude of the non-symmetric force components is significantly lower than the vertical component of the force, with the ring-frequency as the only exception.

Deng et al. (2016) concludes that the non-uniformity of the load is strongest around the ring frequency for an inclined load. The results presented here agree with that, and the same conclusion holds for a force moment on top of the pile.

Fig. 4 compares the peak pressure and sound exposure levels of the inclined and eccentric loads with the vertical load. Despite different approaches, the sound exposure levels and peak pressure levels compare well to Deng et al. (2016) for the symmetric force, i.e. $L_{\text{Peak}} = 198$ dB and $L_{\text{E}} = 177$ dB at $r = 20$ m. The levels are taken at the worst azimuth; thus, either $\theta = 0$ or $\theta = \pi$ dependent on the phase of the forces. As expected from the sound pressure levels, the sound exposure and peak pressure levels are all very close. Especially, the sound exposure levels seem uninfluenced, but the peak pressure levels are all within 1 dB as well.

Deng et al. (2016) state that underwater noise measurements at one location around the circumference are insufficient when the impact force has a significant non-symmetric component. This work supports this statement if one is interested in detailed frequency content around the ring frequency. The differences around the circumference are insignificant if one is interested in more general sound levels, such as the peak pressure and sound exposure levels. Other uncertainties, such as bathymetry variation or seabed composition with strong azimuthal dependence, likely influence sound variations around the azimuthal direction more.

3.2. Large diameter pile

The effects of non-symmetric forces for a large-diameter monopile are studied based on the case of a windmill installed in the German North Sea presented by Peng et al. (2021a). First, the case of the pile driven as described is examined; after that, the pile penetration depth and the impact duration are changed. The pile is eight m in diameter and 76.9 m in length. The soil consists of a thin upper layer founded on the bottom sediment. The material and geometry parameters are given in Table 2. The ring frequency of the pile is 216 Hz, and the fluid cut-off frequency is approximately 9 Hz.

Table 2
Large diameter pile geometry and material properties (Peng et al., 2021a).

Parameter		unit
Pile Youngs modulus [E_p]	210	GPa
Pile Poison's ratio [ν_p]	0.30	–
Pile density [ρ_p]	7850	kg m^{-3}
Structural damping [ν_p]	0.001	–
Pile length [L_p]	76.9	m
Pile radius [r_p]	4	m
Pile thickness [h_p]	0.09	m
Pile soil penetration	40.1	m
Fluid wave speed [c_f]	1500	m s^{-1}
Fluid density [ρ_f]	1000	kg m^{-3}
Water depth	39.9	m
Soil layer compressional wave speed [$c_{s,p}$]	1560	m s^{-1}
Soil layer shear wave speed [$c_{s,s}$]	94	m s^{-1}
Soil layer density [ρ_p]	1670	kg m^{-3}
Soil layer thickness	1.5	m
Soil bottom compressional wave speed [$c_{s,p}$]	1979	m s^{-1}
Soil bottom shear wave speed [$c_{s,s}$]	349	m s^{-1}
Soil bottom density [ρ_p]	1950	kg m^{-3}

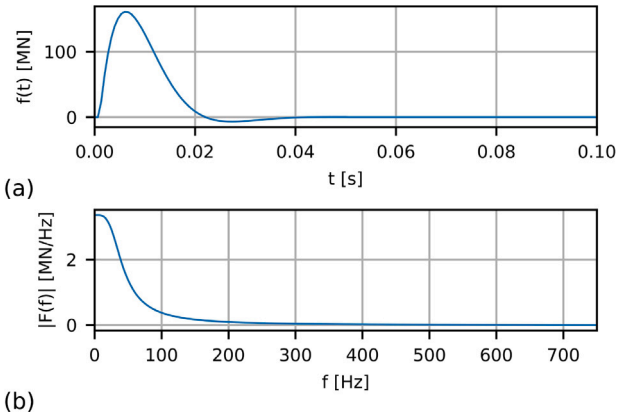

Fig. 5. (a) Time and (b) frequency domain representation of the force on the large-diameter pile (Peng et al., 2021a).

The force on top of the pile corresponds to a hammer blow of approximately 1750 kJ and is described by:

$$F_{\text{ext}}(t) = F_A \sin\left(F_B(t - t_0)\right) \exp^{-F_c(t-t_0)} \qquad t_0 < t < t_1 \tag{14}$$

The force parameters are: $F_A = 503$, $F_B = 149$, $F_c = 150$, $t_0 = 0.001$ s and $t_1 = 0.05$ s, i.e. the force plotted in Fig. 5 with the accompanying Fourier amplitude spectrum. For the analysis, frequencies up to 750 Hz are included with a step of 1 Hz. Fig. 5 shows that the described force contains less high-frequency content than the force applied on the small-diameter monopile, which justifies the upper limit frequency truncation.

Fig. 6 shows the absolute value of the transfer functions and the sound pressure levels corresponding to the case. Similar to the small-diameter monopile, negligible sound is propagated around the ring frequency of the pile due to an axisymmetric vertical load. On the other hand, the absolute value of the transfer function of the horizontal load peaks around these frequencies. This is because the modal density at the first azimuthal mode is high and contains many modes governed by shear motion. Examining the sound pressure levels in Fig. 6b, the noise generated by the horizontal or moment component of the force is significantly smaller at all frequencies except around the ring frequency. This phenomenon is the same at both small- and large-diameter monopiles.

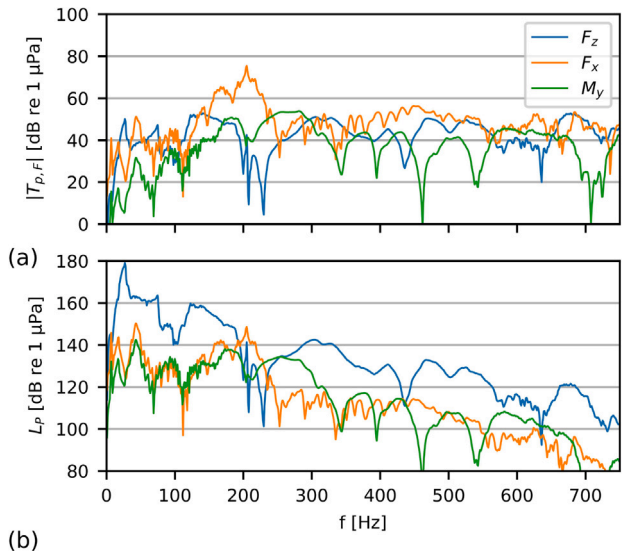

Fig. 6. (a) Absolute value of the transfer functions and (b) sound pressure levels for a vertical load, horizontal load and moment on top of the pile at $z = 20$ m and $r = 100$ m.

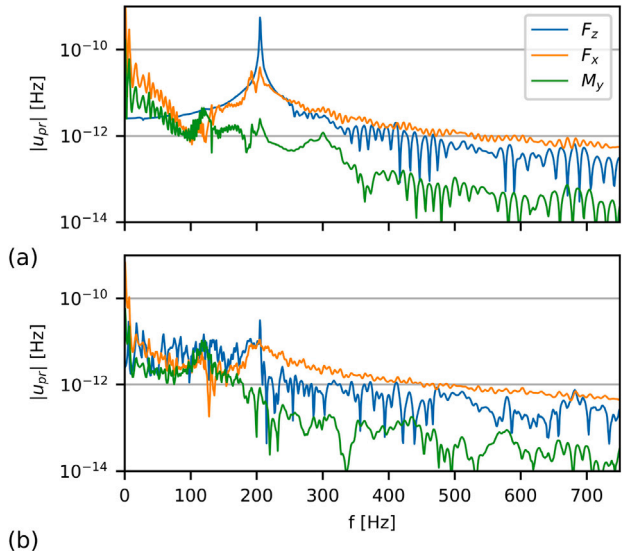

Fig. 7. Absolute value of the transfer functions of the absolute radial pile displacement (a) 0.5 m below the top of the pile and (b) in the centre of the fluid column ($z = 20$).

The ring frequency explains the drop in the noise levels at axisymmetric vertical excitation, while the waves excited around the ring frequency have a vertical group velocity approaching zero. Therefore, energy cannot propagate through the pile and remains close to the hammer impact location. This can be observed by comparing the radial pile vibrations at multiple locations along the pile length around these frequencies.

Fig. 7a shows that the radial displacements peak around the ring frequency at the top of the pile due to a high modal density and little energy propagating downwards. Therefore, this peak is not observed anymore halfway through the fluid column in Fig. 7b.

The horizontal load and moment do not excite horizontal motion around the ring frequency since this mode does not exist in non-symmetric configurations. The largest radial vibrations are observed at low frequencies, where the first bending modes are located (the first between 1.4 and 8.3 Hz assuming fixed-free and free-free boundary conditions, respectively). However, the first bending modes do not cause significant sound levels, as seen in Fig. 6, while the fluid pressure is proportional to acceleration that scales quadratically with frequency.

Fig. 8 shows the time response at $\theta = 0$ for each component of the force individually. It should be stressed that the scales of the horizontal and moment components are 20 times smaller than the colour scale of the vertical component. The vertical force induces a Mach-cone wave that reflects up and down, as indicated with the arrows at 0.02 s and 0.04 s. The noise generation mechanism and the angle of the Mach-cone, $\phi = \sin^{-1}\left(c_f/c_{p,p}\right) \approx 17°$, are in agreement with theory (Reinhall and Dahl, 2011), with $c_{p,p}$ corresponding to the compressional wave speed of the pile. Furthermore, at $t = 0.08$ s, Scholte interface waves are visible in the wave field.

The noise generation mechanism due to a horizontal load or moment varies from the case of a vertical load. At $t = 0.02$ s, two Mach-cones are identifiable, as the arrows indicate.

The second Mach-cone is active by the slower travelling shear wave with a shorter length. The shorter wavelength is clearly observable at 0.03 s, where the positive and negative pressure levels along the pile alter more quickly than the field generated by a vertical load. It also shows that sound is radiated along a longer timespan.

The Mach-cone generated by the shear wave has an angle of $\phi = \sin^{-1}\left(\frac{c_f}{c_{p,s}}\right) \approx 27°$, in which $c_{p,s}$ refers to the shear-wave velocity of the pile. The transmission loss model presented by Lippert et al. (2018) shows a relation between the propagation angle of the wave and transmission losses. The Mach waves with an angle of 27° are expected to propagate less efficiently due to a larger number of reflections with the seabed and a smaller reflection coefficient due to a greater angle between water and soil. Therefore, at more considerable distances, the contribution of the non-symmetrical components of the noise field will be less prominent than in the near field. Depending on the water depth and the reflection coefficient of the seabed, the added transmission loss is more or less significant.

Scholte interface waves at the seabed are less prominent because the horizontally dominated pile vibrations excite Love waves. The latter does not cause noise into the fluid domain because they have no vertical component in the displacement field and contain only horizontally polarized shear waves (SH waves).

In practice, the peak pressure and sound exposure levels are usually reported and checked against noise thresholds imposed by regulators. Fig. 9 shows that the non-symmetric components do not influence noise levels at the critical azimuth ($\theta = 0$ or $\theta = \pi$). This aligns with the observations of the sound pressure levels; the horizontal load and moment only contribute around the ring frequency, and there is little energy at these frequencies. Besides that, it should be remembered that waves at a particular frequency rarely fully sum up because of a phase difference. Furthermore, it can be concluded that an inclined load causes higher noise levels than an eccentric load, though both are insignificant in this case. These conclusions can alter if the force has more energy around the ring frequency or when the system properties change. Both cases are examined hereafter.

3.2.1. Variation of the pile penetration depth

In impact pile driving, the hammer energy to drive the pile usually increases with the pile penetration depth in cases with relatively homogeneous soil. Therefore, the deeper pile penetration depths are often critical in noise predictions. However, this statement might deviate for inclined and eccentric loads. Fig. 10 shows the sound pressure levels around three pile penetration depths, assuming the same force. It is observed that the three lines in the same colour in all cases are comparable and mostly overlap. Therefore, the effect of inclination and eccentricity of the force is expected to be similarly small throughout the driving process.

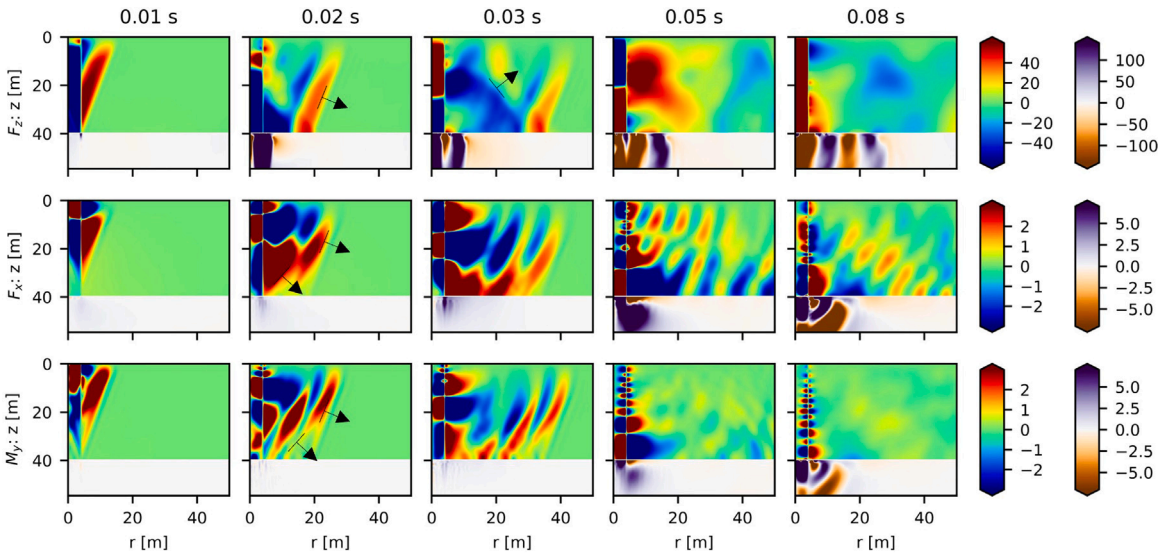

Fig. 8. 2D time response at $\theta = 0$ of fluid pressure [kPa] and vertical soil velocity [mm s^{-1}] due to a vertical, horizontal and moment load on top of the pile at five subsequent time moments.

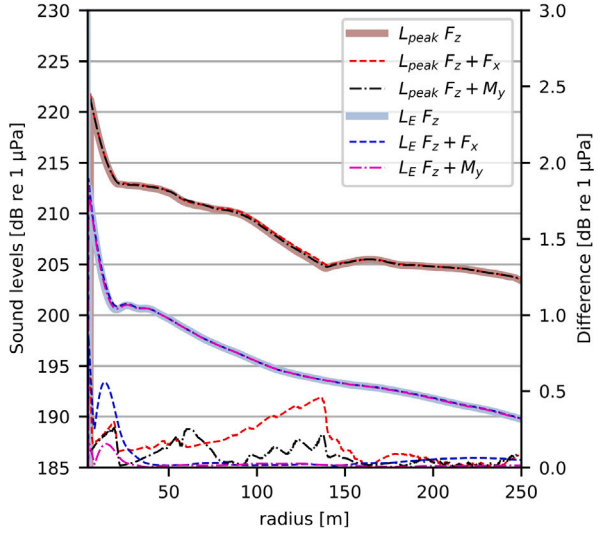

Fig. 9. Peak pressure and sound exposure levels at $z = 35$ m to radius caused by the vertical, inclined, and eccentric load on the left axis and the difference to only the vertical load on the right axis.

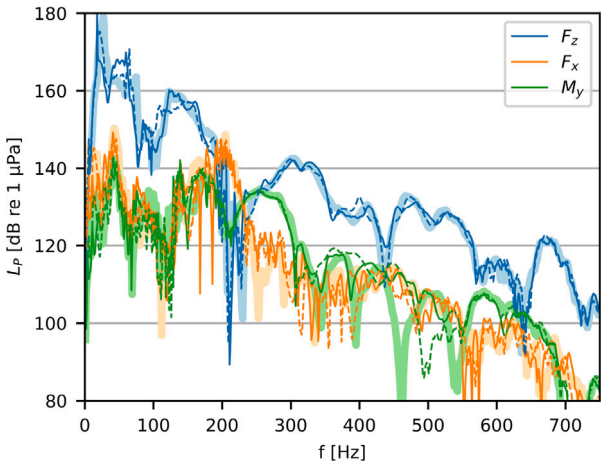

Fig. 10. Sound pressure levels per force component at $z = 20$ m and $r = 100$ m around three pile penetration depths: 19.9 m - solid, 29.9 m - dashed, and 39.9 m - light and thick.

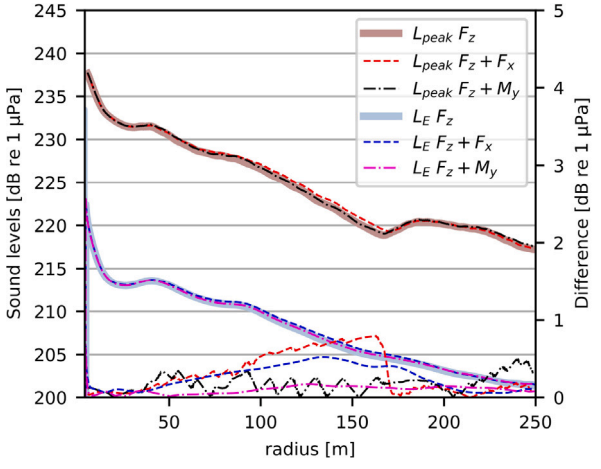

Fig. 11. Peak pressure and sound exposure level at $z = 35$ m for a vertical, inclined, and eccentric load and on the left axis the differences compared to the vertical load on the right axis.

3.2.2. Shorter impact duration

The hammer impact presented by Peng et al. (2021a) has relatively little energy at the ring frequency. A case with more energy around the ring frequency can alter previous observations. Therefore, the pulse duration is four times shortened. At the same time, the amplitude is proportionally enlarged to keep the same energy in the hammer blow but with higher frequency content in the amplitude spectrum.

Fig. 11 shows the resulting sound exposure and peak pressure levels. Both levels have increased due to the shorter duration of the pulse. The effect of inclination or eccentricity is slightly higher, but still in all cases below 1 dB within the first 250 m. Thus, due to an impact force with more energy around the ring frequency, the effect of inclination and eccentricity of the force is larger but still limited.

3.3. Inclined pile

This section describes the sound generation of a slightly inclined pile, with a hammer force in parallel with the pile. The case refers

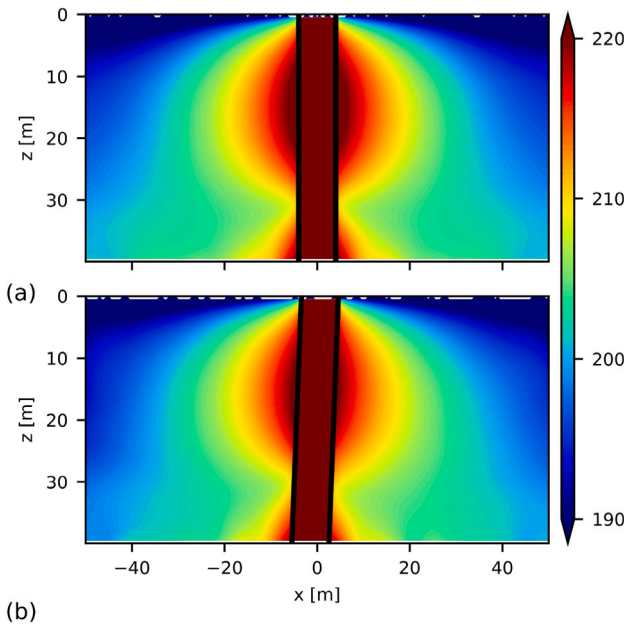

Fig. 12. Sound exposure levels of the vertical pile (a) compared with the incline pile (b).

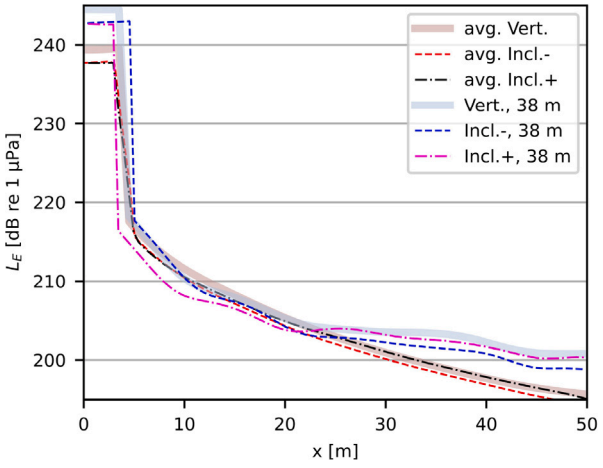

Fig. 13. Sound exposure levels to the distance at $z = 38$ m and averaged over the fluid column for the vertical and inclined piles. The + and − refer to the positive and negative x-coordinate, respectively.

to unintended tilting of the pile during the installation of monopile foundations. This particular scenario may occur at the initial stages of a pile-driving process. The effect of pile inclination is examined by considering an extreme case where a large-diameter monopile is inclined at an angle of three degrees at $z_2 = 50$ m. A 3D Comsol Multiphysics model is used for the study, where symmetry around $y = 0$ is applied to reduce the model size. However, the computational considerations lead to the truncation of the domain at $r = 50$ m and the frequencies at $f = 400$ Hz.

Fig. 12 presents the comparison of SEL for a vertical pile (a) and an inclined pile (b). Upon initial observation, the inclination appears to have a negligible impact on SEL. Both cases exhibit similar spatial distributions and amplitudes. However, slight variations between positive and negative x-coordinates are observed in Fig. 12b, particularly above the seabed.

Examination of Fig. 13 confirms the slight variation in SEL between positive and negative x-coordinates. The variation is the largest close

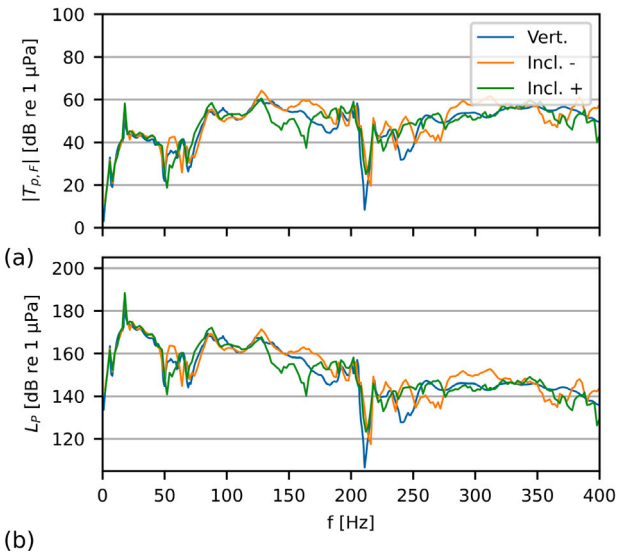

Fig. 14. Absolute value of the transfer functions and sound pressure levels at $x = +/-40$ m and $z = 20$ m for the vertical and inclined pile.

to the pile, just above the seabed, as visually observed in Fig. 12. The variation on both sides is in the first 10 m up to 5 dB. However, at a slightly larger distance (>20 m), SELs converge with a maximum variation of 2 dB. The differences on both sides are largest due to the presence of the seabed. The average SEL over the water depth shows significantly less variation on both sides. SEL stay within 2 dB.

In both cases, the SEL values are higher at positive x-coordinates, i.e., the side where the top of the pile leans. This can be explained by additional reflections caused by the smaller angle between the pile and soil compared to the negative x-coordinate. Though a very conservative case is modelled, noise levels at the positive and negative sides deviate mainly in the vicinity of the pile but up to only two decibels.

In Fig. 14, the frequency distribution of the generated noise is analysed through transfer functions and SPLs. The absolute value of the transfer functions, which describe the system behaviour, exhibit similar trends in inclined and vertical pile cases. The absolute value of the transfer functions for the inclined pile at positive and negative x-coordinates fluctuates around the function belonging to the vertical pile. When multiplied by the force function, the SPL presented in Fig. 14b peaks at 18 Hz, which dominates the SEL above. The substantial decrease in noise at the ring frequency indicates that the pile mainly vibrates at its cylindrically symmetric modes excited by the aligned hammer force despite the non-symmetric geometric coupling with fluid and soil.

Fig. 15 shows a snapshot of the emitted noise field after 0.03 s. The primary noise generation mechanism in the inclined pile is similar to the vertical pile, the Mach wave radiation. Next, the surface wave is generated along the seabed. The vertical soil vibrations are excited along the inclined surface of the pile. Nonetheless, seabed vibrations do not deviate significantly on both sides of the pile.

The primary noise generation mechanism can explain the minor changes in observed frequency domain pressure fields since there is a significant difference on both sides of the pile, namely, the angle of the Mach cones with the seabed. Due to the inclination of the pile of three degrees, the Mach cones have a rotated angle of three degrees compared to the vertical pile. The Mach wave with an angle of 14 and 20° will have fewer and more reflections at some horizontal distance, respectively, with the seabed compared to the Mach wave from the vertical pile. This will affect the transmission losses over large distances. The significance of the effect on the transmission loss depends on the reflection coefficient of the sediment and the water depth (Lippert et al., 2018).

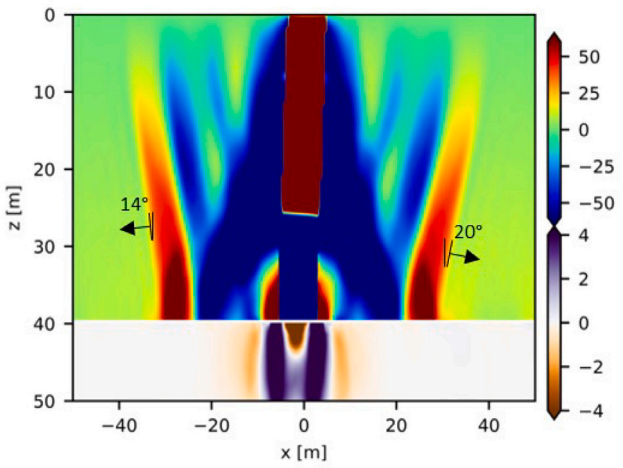

Fig. 15. Snapshot of the fluid pressure [kPa] and vertical soil velocity [mm s^{-1}] at $y = 0$ m and $t = 0.03$ s.

The presented results do not provide conclusive evidence that inclination plays an insignificant role in noise prediction, given that slight variations of one decibel can be significant in underwater noise predictions. Slightly higher noise levels are observed on the side where the top of the pile leans; however, it remains inconclusive if these observations hold at more considerable distances. Regardless, it can be indicated that even with a more considerable inclination at the beginning of piling, the tip of the pile does not significantly alter the results obtained for a vertical pile, considering the allowable inclination at the end of the driving process is 0.25 degrees.

4. Conslusion

This study investigates the impact of non-symmetric impact forces and pile inclination on underwater noise for small- and large-diameter monopiles cases. Specifically, the study examines the case of an inclined and eccentric force and a tilted pile. First, the response to the non-symmetric forces is studied. The absolute value of the transfer functions of the horizontal force and moment are comparable to or larger than those of the vertical force. However, the vertical component generates most underwater noise due to a much higher force amplitude. The inclined force produces slightly higher noise levels than the eccentric force. Still, the increased sound levels seem insignificant, even at the least favourable azimuth, since more likely factors to occur are introducing small variations of the sound exposure levels, such as a strike-to-strike variation. Nevertheless, in some cases, half a decibel can be decisive in crossing allowable thresholds.

Non-symmetries strongly affect only the sound pressure levels around the ring frequency of the pile. The drop in sound pressure levels around the ring frequency for a purely vertical load disappears when a non-symmetric component is present. Furthermore, seabed vibrations are barely induced by inclined and excentric forces, while these forces excite Love waves instead of Rayleigh waves. Based on the presented cases, inclined or eccentric forces should be examined when:

- there is a strong interest in the frequency distribution of the noise levels; for example, to examine noise levels for species sensitive to the noise around the ring frequency of the pile,
- The excitation force contains significant energy around the ring frequency, for example, when a vibratory hammer is used with energy in the ring frequency through its driving frequency or superharmonic.

Nevertheless, the inclination or eccentricity of an impact hammer on top of the pile is unlikely to significantly affect noise levels in most cases since the conclusions could be generalized for all pile sizes, pile penetration depths, and impact duration studied in this work.

An inclined pile radiates a comparable noise field as the vertical pile, generated mainly by Mach wave radiation and Scholte interface waves. Due to the inclination of the pile in its surroundings, slightly higher noise levels are observed at the side of the pile with a smaller angle with the seabed. In the far field, the rotation of the Mach cone may affect the measured noise levels. Nonetheless, sound level variations in the near field were relatively small, especially considering the large inclination assumed in the analysis.

CRediT authorship contribution statement

Timo Molenkamp: Conceptualization, Formal analysis, Investigation, Methodology, Validation, Visualization, Writing – original draft. **Apostolos Tsouvalas:** Supervision, Writing – review & editing. **Andrei Metrikine:** Funding acquisition, Supervision, Writing – review & editing.

Declaration of competing interest

The authors declare the following financial interests/personal relationships which may be considered as potential competing interests: Timo Molenkamp reports was provided by Delft University of Technology.

Data availability

No data was used for the research described in the article.

Acknowledgements

This paper is associated with the GDP project in the framework of the GROW joint research program. Funding from *Topsector Energiesubsidie van het Ministerie van Economische Zaken* under grant number TEHE117100 and financial/technical support from the following partners is gratefully acknowledged: Royal Boskalis Westminster N.V., CAPE Holland B.V., Deltares, Delft Offshore Turbine B.V., Delft University of Technology, ECN, Eneco Wind B.V., IHC IQIP B.V., RWE Offshore Wind Netherlands B.V., SHL Offshore Contractors B.V., Shell Global Solutions International B.V., Sif Netherlands B.V., TNO, and Van Oord Offshore Wind Projects B.V.

References

COMSOL Multiphysics®, 2022. COMSOL Multiphysics® V. 6.1. COMSOL AB, Stockholm, Sweden, www.comsol.com.

Dahl, P.H., Reinhall, P.G., Popper, A.N., Hastings, M.C., Ainslie, M.A., 2014. Underwater sound from pile driving, what is it and why does it matter. J. Acoust. Soc. Am. 135 (4), 2312. http://dx.doi.org/10.1121/1.4877620.

Deng, Q., Jiang, W., Tan, M., Xing, J.T., 2016. Modeling of offshore pile driving noise using a semi-analytical variational formulation. Appl. Acoust. 104, 85–100. http://dx.doi.org/10.1016/j.apacoust.2015.11.002.

Fricke, M.B., Rolfes, R., 2015. Towards a complete physically based forecast model for underwater noise related to impact pile driving. J. Acoust. Soc. Am. 137 (3), 1564–1575. http://dx.doi.org/10.1121/1.4908241.

Göttsche, K.M., Steinhagen, U., Juhl, P.M., 2015. Numerical evaluation of pile vibration and noise emission during offshore pile driving. Appl. Acoust. 99, 51–59. http://dx.doi.org/10.1016/j.apacoust.2015.05.008.

ISO, 2017. ISO 18405:2017 underwater acoustics — Terminology. URL https://www.iso.org/standard/62406.html.

Jestel, J., von Pein, J., Lippert, T., von Estorff, O., 2021. Damped cylindrical spreading model: Estimation of mitigated pile driving noise levels. Appl. Acoust. 184, 108350. http://dx.doi.org/10.1016/j.apacoust.2021.108350.

Jiang, Q., Wang, X., Yu, M., Tang, M., Zhang, H., Wu, J., 2022. Theoretical study of vibro-acoustics of fluid-pile-soil coupled system and experimental research of noise reduction of small-scale pile driving. Ocean Eng. 252 (February), 110997. http://dx.doi.org/10.1016/j.oceaneng.2022.110997.

Leissa, A.W., 1973. Vibration of Shells. Technical Report, Scientific and Technical Information Office National Aeronautics and Space Administration, Washington, D.C., p. 428.

Lippert, T., Ainslie, M.A., von Estorff, O., 2018. Pile driving acoustics made simple: Damped cylindrical spreading model. J. Acoust. Soc. Am. 143 (1), 310–317. http://dx.doi.org/10.1121/1.5011158.

Lippert, T., Lippert, S., 2012. Modelling of pile driving noise by means of wavenumber integration. Acoust. Aust. 40 (3), 178–182.

Lippert, S., Nijhof, M., Lippert, T., Wilkes, D., Gavrilov, A., Heitmann, K., Ruhnau, M., von Estorff, O., Schafke, A., Schafer, I., Ehrlich, J., MacGillivray, A., Park, J., Seong, W., Ainslie, M.A., de Jong, C., Wood, M., Wang, L., Theobald, P., 2016. COMPILE—A generic benchmark case for predictions of marine pile-driving noise. IEEE J. Ocean. Eng. 41 (4), 1061–1071. http://dx.doi.org/10.1109/JOE.2016.2524738.

Madsen, P., Wahlberg, M., Tougaard, J., Lucke, K., Tyack, P., 2006. Wind turbine underwater noise and marine mammals: implications of current knowledge and data needs. Mar. Ecol. Prog. Ser. 309 (Tyack 1998), 279–295. http://dx.doi.org/10.3354/meps309279.

Molenkamp, T., Tsouvalas, A., Metrikine, A., 2023. The influence of contact relaxation on underwater noise emission and seabed vibrations due to offshore vibratory pile installation. Front. Mar. Sci. 10 (March), 357. http://dx.doi.org/10.3389/FMARS.2023.1118286.

von Pein, J., Lippert, T., Lippert, S., von Estorff, O., 2022. Scaling laws for unmitigated pile driving: Dependence of underwater noise on strike energy, pile diameter, ram weight, and water depth. Appl. Acoust. 198, 108986. http://dx.doi.org/10.1016/j.apacoust.2022.108986.

Peng, Y., Tsouvalas, A., Stampoultzoglou, T., Metrikine, A.V., 2021a. A fast computational model for near- and far-field noise prediction due to offshore pile driving. J. Acoust. Soc. Am. 149 (3), 1772–1790. http://dx.doi.org/10.1121/10.0003752.

Peng, Y., Tsouvalas, A., Stampoultzoglou, T., Metrikine, A.V., 2021b. Study of the sound escape with the use of an air bubble curtain in offshore pile driving. J. Mar. Sci. Eng. 9 (2), 232. http://dx.doi.org/10.3390/jmse9020232.

Reinhall, P.G., Dahl, P.H., 2011. Underwater Mach wave radiation from impact pile driving: Theory and observation. J. Acoust. Soc. Am. 130 (3), 1209–1216. http://dx.doi.org/10.1121/1.3614540.

Southall, B.L., Finneran, J.J., Reichmuth, C., Nachtigall, P.E., Ketten, D.R., Bowles, A.E., Ellison, W.T., Nowacek, D.P., Tyack, P.L., 2019. Marine mammal noise exposure criteria: Updated scientific recommendations for residual hearing effects. Aquat. Mamm. 45 (2), 125–232. http://dx.doi.org/10.1578/AM.45.2.2019.125.

Sunday, K., Brennan, F., 2021. A review of offshore wind monopiles structural design achievements and challenges. Ocean Eng. 235 (June), 109409. http://dx.doi.org/10.1016/j.oceaneng.2021.109409.

Tsetas, A., Tsouvalas, A., Gómez, S.S., Pisanò, F., Kementzetzidis, E., Molenkamp, T., Elkadi, A.S., Metrikine, A.V., 2023. Gentle driving of piles (GDP) at a sandy site combining axial and torsional vibrations: Part I - installation tests. Ocean Eng. 270 (April 2022), 113453. http://dx.doi.org/10.1016/j.oceaneng.2022.113453.

Tsouvalas, A., 2020. Underwater noise emission due to offshore pile installation: A review. Energies 13 (12), 3037. http://dx.doi.org/10.3390/en13123037.

Tsouvalas, A., Metrikine, A.V., 2013. A semi-analytical model for the prediction of underwater noise from offshore pile driving. J. Sound Vib. 332 (13), 3232–3257. http://dx.doi.org/10.1016/j.jsv.2013.01.026.

Tsouvalas, A., Metrikine, A.V., 2014. A three-dimensional vibroacoustic model for the prediction of underwater noise from offshore pile driving. J. Sound Vib. 333 (8), 2283–2311. http://dx.doi.org/10.1016/j.jsv.2013.11.045.

Veritas, D.N., 2004. Design of offshore wind turbine structure.

Wilkes, D.R., Gavrilov, A.N., 2017. Sound radiation from impact-driven raked piles. J. Acoust. Soc. Am. 142 (1), 1–11. http://dx.doi.org/10.1121/1.4990021.

Zampolli, M., Nijhof, M.J.J., de Jong, C.A.F., Ainslie, M.A., Jansen, E.H.W., Quesson, B.A.J., 2013. Validation of finite element computations for the quantitative prediction of underwater noise from impact pile driving. J. Acoust. Soc. Am. 133 (1), 72–81. http://dx.doi.org/10.1121/1.4768886.